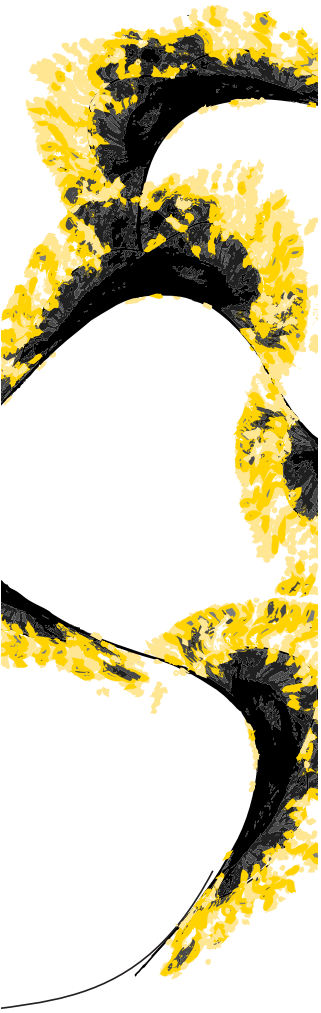

RAM ROBOTICS AND MECHATRONICS

DEMONSTRATION OF A MULTI-AXIS STEPPER MOTOR IN A ROBOTIC SYSTEM

C. (Christiaan) Muetstege

BSC ASSIGNMENT

Committee:
prof. dr. ir. L. Abelmann
dr. V. Groenhuis, MSc
dr. ir. J.J. de Jong

February, 2022

011RaM2022
Robotics and Mechatronics
EEMathCS
University of Twente
P.O. Box 217
7500 AE Enschede
The Netherlands

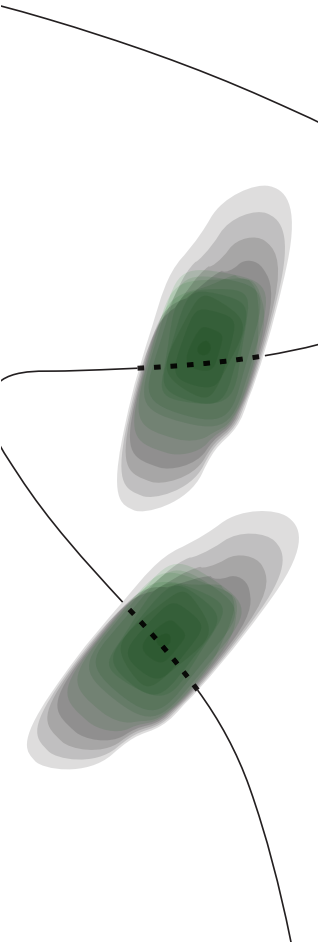

UNIVERSITY OF TWENTE. | TECHMED CENTRE UNIVERSITY OF TWENTE. | DIGITAL SOCIETY INSTITUTE

Abstract

This report describes the design and creation of a parallel manipulator for the task of launching a ping pong ball, designing the PM and setting up simplified equations. The physical version is compared to a model, to find components that should have been modelled to understand the launch better, the operating limits are discussed, and some optimisation is discussed.

Table of Contents

I. Introduction

In the world of robotics there are so called manipulators, these robots are specialised in moving something from a to b at high speeds accurately or for example have a tool mounted to their end effector which they can orient very precisely and accurately. These manipulators come in many versions, the basic division is done in the two groups “Parallel” and “Serial” as seen in Figure 1.

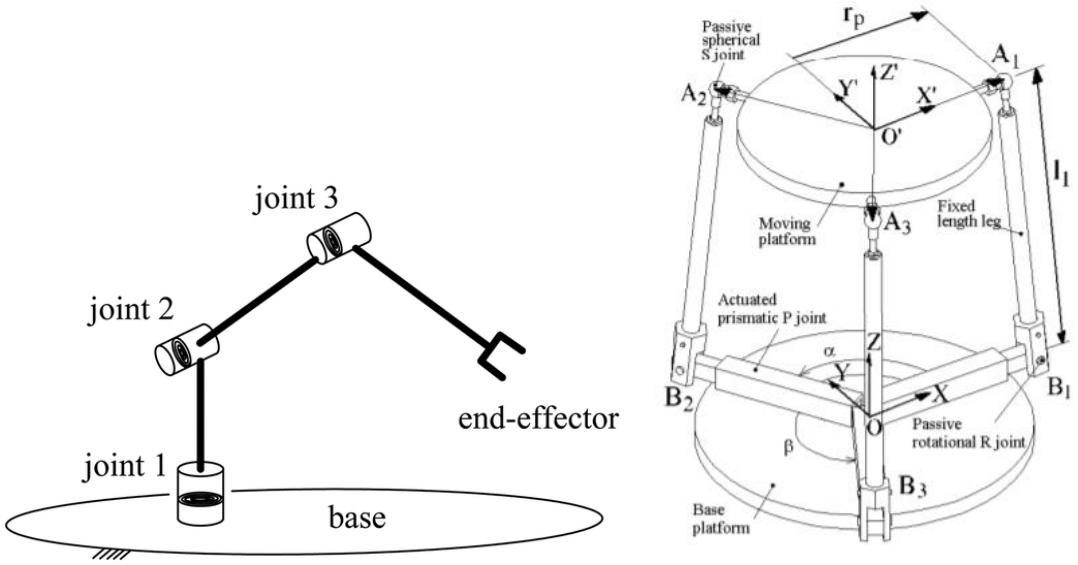

Figure 1 a: 3-R serial manipulator [4], b: 3-PRS parallel manipulator [3]

These manipulators are used in many situations where people are not precise, strong or fast enough, where people couldn’t be in the first place or as a cheaper alternative.

The difference between these types is that in a serial manipulator each stage is only connected to the previous and the next by one joint [7], these however are less sturdy at the end effector due to the end effector being connected to the base through a set of moments. These manipulators are not always supposed to be perfectly positioned and solid, in some cases where there is risk of damage compliant serial manipulators can be used [4].

This paper however will focus on the design of a non-compliant parallel manipulator. In a parallel manipulator (PM) the end effector (or platform) is connected to by multiple joints or series of joints which together create a stronger more stable end effector. Parallel manipulators come in many degrees of freedom with varying types and numbers of joints and with different

driven joints, in figure 1b the driven joints are the prismatic joints (B), but other PMs exist where the basic setup is the same only differing in the orientation of the prismatic joints [8]. When looking at other PM's [6] the driven joint could also be a prismatic joint replacing the fixed arms (I). The first approach as shown in figure 1b and variations [5] seems to be more popular for analysis [3] and creation [2].

In this report the goal will be to create a parallel manipulator using a novel multi-axis electric stepper motor, Figure 2, And whether it is able to launch a ball. The unique coaxial setup of the multi-axis motor could be used to drive the three prismatic joints in Figure 1b (B1, B2, B3) with a rack and pinion setup, this would allow for the creation of a PM due to the motors ability to drive all three linear motions by itself. This would create a tri-glide parallel manipulator [2] on a smaller scale due to the ability to place the motor in the centre as opposed to on the outside of each linear slider as in a tri-glide when motorising a PM.

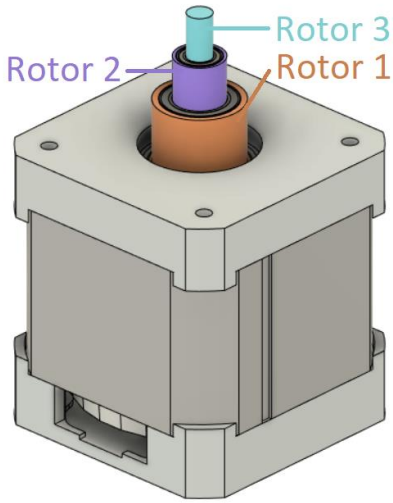

Figure 2: Multi-axis electric stepper motor

The motor is to put is simply a stack of three smaller stepper motors combined in the same housing which makes it super compact, it is very important to note that not all rotors behave the same. The rotors all have a slight variation in the number of steps per rotation, also with slight variations in torque as well as slightly varying maximum velocities [1]. To fully understand the launch of the ball or the lack thereof behaviour of the platform will be related to these motors specifications to apply in a model which can then be compared to video measurements of the physical version, retrieve the velocity and acceleration and figure out what these mean for launching the ball with this PM.

II. Theory

To launch a ping pong ball with the parallel manipulator (PM) the platform has to be able to reverse accelerate with at least 9.81 m/s^2 to be able to dive under the ball, with the velocity before this reverse acceleration being maximised to maximise the launch height.

A. Multi-axis stepper motor

The multi axis electric stepper motor used in the PM is what enables this design to become a compactor version of a Tri glide PM [2]. The stepper motor drives the three axes coaxially, to achieve this while retaining full control over each rotor and preventing rotor dependencies, all three rotors have a different number of steps per rotor [1]. The motor position is determined with electric radians, this describes the electrical signal used to drive the motor. The relation between the electric radians and the radians of the rotors are the number of steps the rotor has. Converting electric radians to radians the value has to be divided by the number of teeth in the motor. This means that the targeted number of radians is set by multiplying it by the array [44,46,48] the number of steps for rotors 1, 2 and 3 respectively. This array is used for setting the acceleration, the velocity and the position so all three rotors have equal behaviour.

B. Design

The PM build will be a tri-glide parallel manipulator, this design is driven by 3 linear motions rotated with *120°* separation, this PM is very suited to be driven by the multi-axis stepper motor due to the three linear motions being easily made using a rack and pinion setup for each of the motor's axes. This is an alternative to a three motor (or hand driven [2]) setup.
The tri-glide parallel manipulator is a 3-PRS parallel mechanism, with three different types of joints with different constraints. The first in the drive chain is a prismatic joint (P) which has one translational freedom without rotation (J1 in Figure 3).

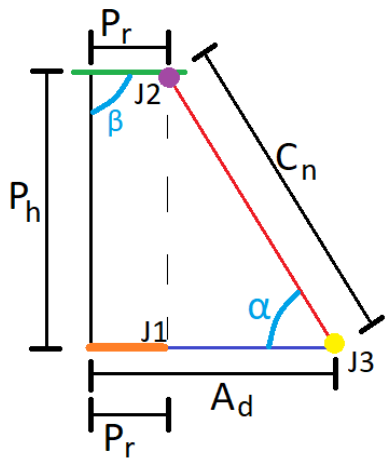

Figure 3: Schematic of basic analysis of the physical design

The second is a revolute joint (R) with one rotational freedom without translation (J3). The third is the spherical joint (S) which allows for three rotational freedoms and no translational (J2).

The first physical version of the design is shown in Figure 4, it shows a single layer (bottom layer) consistent with the rack, pinion and the bottom housing, this housing is larger as it is also the motor mount. Three of these layers are stacked at rotated intervals of *120°* with the pinion inner diameters decreasing to fit the axes and the housing altered each level to not interfere with other levels. In the second version the decision was made to make the housings triangle shaped instead of square to prevent the interference with the other levels.

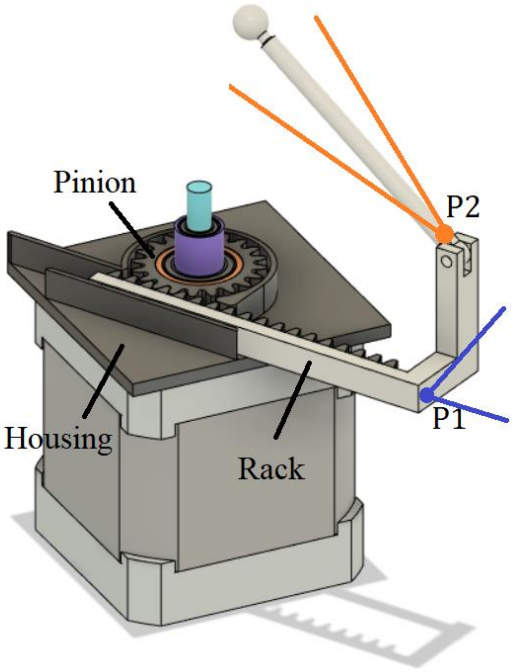

Figure 4: 3D design of the first PM iteration

C. Design improvements

In Figure 5 the design is shown for the stability improved PM, this time with an extra guide for the driving arm to prevent the blue parasitic rotation around (P1) shown in Figure 4. Also replacing the single revolute joint with a spaced double revolute joint to prevent the parasitic rotational motion around (P2). Other changes are the extension of the rack (R) to prevent the rack from binding at the back of the housing, a lengthened guide for the rack and a slight offset for hinge tower (T) to retain part of the maximum displacement lost by the housing size increase as well as clearing space for the new additional guide.

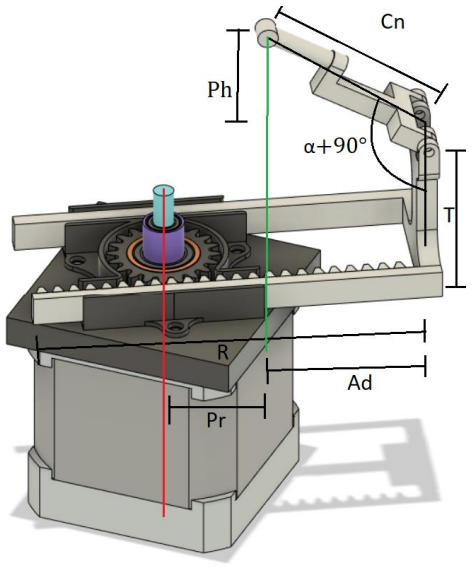

Figure 5: 3D design of a single arm of the parallel manipulator

D. Motor to driving arm

To turn the three rotational freedoms of the motor into the three translational freedoms used for the tri-glide manipulator, three rack and pinion setups are used. To keep the PM small a pinion size of 10 mm is chosen for S_{rw} (real pinion radius), since this would result in an acceleration of 20 m/s^2 in combination with the motors acceleration of 2000 rad/s^2 [1] which should be enough to dive under the ball to create airtime.
The racks are rotated at ⅔π intervals at different heights on the motors separate axes, at the end of these racks are tower offsets so that for all three racks the revolute joints Figure 3 (J3) are at equal height.

E. Driving arm to platform

The platform's relation to the driving arm functions according to the Pythagorean theorem, Figure 3 A_d, C_n and P_h, with a modification to account for the platform angle. A simplified model is made focussing on 1 of the 3 arms, modelling the platform to only modify the platform angle, rotating without translation. Another simple model would be to only model the platform height and making the platform only translational along the Z axis.

The driving arm displacement (A_d), the connector arm length (C_n), platform height (P_h) and platform angle (β) are required to determine the platform height from the arm displacement Figure 3, first the arm offset due to the platform angle has to be determined (O_a) with Equation

2.1 which can then be entered in the Pythagorean theorem resulting in the relation between the arm displacement and the platform height Equation 2.2.

$$O_a = A_d + \cos(\beta) P_r \quad (2.1)$$

$$P_h = \sqrt{C_n^2 - O_a^2} \quad (2.2)$$

For launching the ball, the focus will be on the simplified model for platform height preventing platform rotation by moving all 3 arms equally, since the objective of this paper is to analyse the vertical motion of the platform, the β will be set to π/2 resulting in Equation 2.3 for the platform height.

$$P_h = \sqrt{C_n^2 - A_d^2} \quad (2.3)$$

F. Platform limits

Another element to account for is the driving angle (β), Equation 2.4, this angle decreases with extension of the driving arm which causes the vertical drive efficiency (γ) to be limited as shown in Equation 2.4,

$$\gamma = \sin(\alpha) \quad (2.4)$$

Figure 6 shows the direction and vectorisation of forces resulting in γ and σ in relation to the driving angle α. The other drawn ratio in the figure, σ, is the inward ratio between the force on the arm and the force pointing inward for each of the driving arms, these forces meet in line with the axis of the rotors in equilibrium, cancelling the forces.

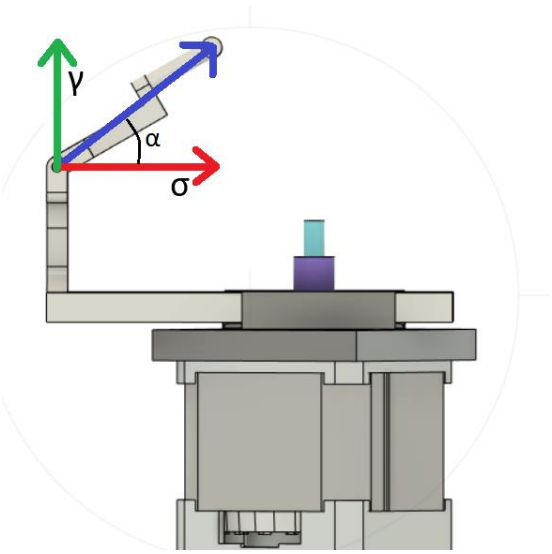

Figure 6: Direction of forces and visual representation of drive efficiency (γ)

When γ is too low the motor will not be able to push the platform up [2], as most of the force is pointing horizontally into the PM. To prevent this a lower boundary for angle α is set at π/6, setting the minimum for γ to be 0.5, so that always at least half the force on the driving arm is transferred to the platform.

For launching a ball there is another concern, the relation between the arm velocity and the platform velocity is dependent on the arm position as can been seen in Equation 2.5 which is the differential of Equation 2.3.

$$\frac{\delta P_h}{\delta t} = \frac{A_d}{\sqrt{C_n^2 - A_d^2}} \tag{2.5}$$

Ad will always be between 0 and Cn with the velocity being the highest when A_d approaches C_n and when approaching 0 the velocity transfer will approach 0. This would call for a higher A_d as this is interesting for launching a ball but does involve a low driving angle and is therefore limited. The highest value A_d should thus take can be found with Equation 2.6.

$$A_d = \cos(\alpha) C_n \tag{2.6}$$

Using the design as shown in Figure 3 this would be a maximum extension of 0.0325 m, combined with the requirement to provide a high enough release velocity the best operation for the PM will be using driving angles between π/3 and π/6 (or arm displacements of 0.0325 m and

0.0188 m) setting the arm operating range to 0.0137 m. Figure 7 the behaviour of the platform when the driving arm velocity is at a constant 1 m/s, including the upper velocity limit π/3 and the lower force limit π/6.

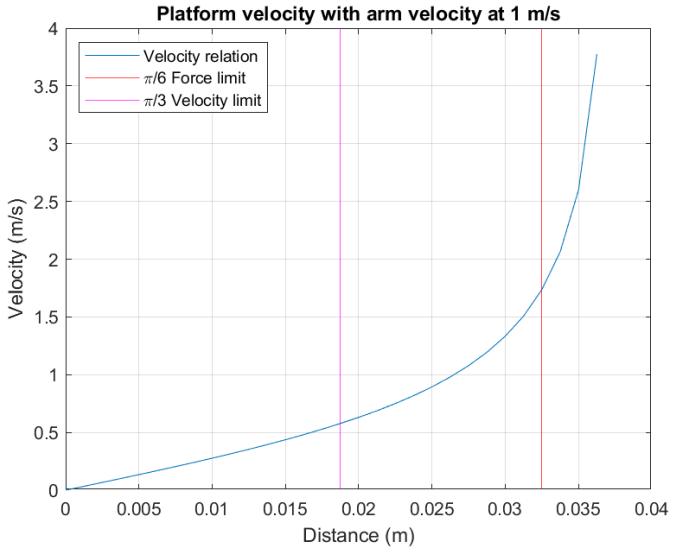

Figure 7: Relation between the driving arm velocity and the platform velocity, With operational boundaries

G. Camera parallax

During the measurements of the platform and the ball a camera will be used to retrieve the position data of the launch. When using a camera for measurement, camera parallax occurs. Camera parallax means that the measured value (P_p) is scaled depending on the distance between the measuring instrument and the measured object (A_a) and the distance between the camera and the measured object (A) as seen from the camera as seen in Figure 8. If this distance is not measured it could lead to a systematic measurement error (e).

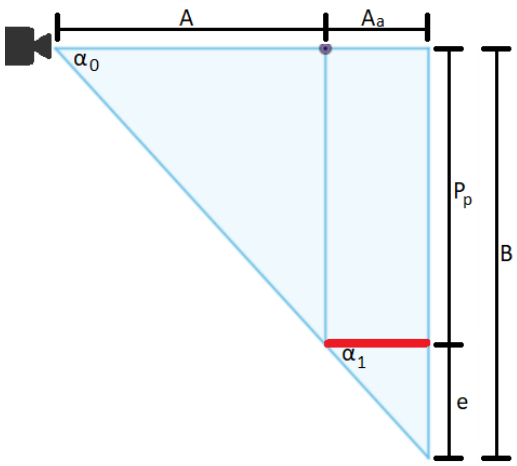

Figure 8: camera parallax of the measurement of the platform (red) with A representing the vertical distance from the camera to the measured object A_a representing the distance between the object and the measurement instrument.

The camera parallax can be calculated using a set of equations, starting with equation 2.7, which sets angles α equal due to the F-angle along the hypotenuse in Figure 8. With equations 2.8 and 2.9 the camera parallax results in equation 2.10. This parallax can then be subtracted from the measurement and re-written to be a multiplication factor.

$$\alpha_0 = \alpha_1 \tag{2.7}$$

$$\alpha = \arctan(\frac{B}{A}) \tag{2.8}$$

$$e = A_a \tan(\alpha) \tag{2.9}$$

$$e = A_a \frac{B}{A} \tag{2.10}$$

$$P_p = B - A_a \frac{B}{A} = B(1 - \frac{A_a}{A}) \tag{2.11}$$

To determine the best fitting ruler distance (A_a) for the measurement the least sum of squares is used on the platform measurement and the platform simulation. This distance is then used for the measurement parallax for both the measured platform adjustment and the measured ball adjustment.

III. Method

To determine whether the platform velocity and acceleration are sufficient to launch the ping pong ball both a model and a physical version are made. For measuring the platform and ball movement, a Samsung Galaxy s7 (SM-G930F) is used with slow motion capture at 240 frames per second. After the data is collected from the video measurement and the MATLAB simulation, for both the platform and the ball, the measured versus simulated results are compared.

A. Video measurement

For the video measurement the phone is mounted to the table and parallel to the PM a ruler is placed vertically on the side of the image. A ruler overlay is added in post with known distances based on the recorded ruler, and a frame counter is also added which can be seen in Figure 9. For the video measurements it is important to have high contrast between the target object and the background to be able to identify the distinct values properly.

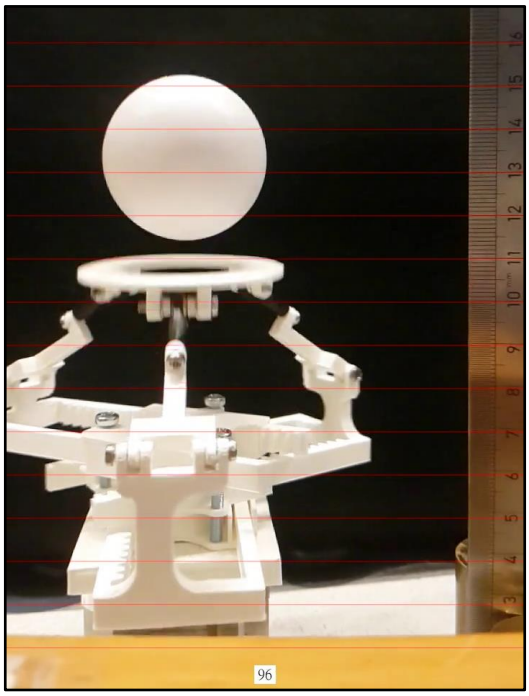

Figure 9: Video measurement of setup with ruler, with bottom frame counter and red overlay matching ruler (red).

The platform and the ball will be measured frame by frame at their top, for the ball this has to be offset to the height where it contacts the platform for equal comparison. As for the motor the maximum velocity will be set to *39* rad/s with an acceleration of *1083* rad/s^2.

The video measurement of the position of the platform will be converted to data by examining the video frame by frame and in combination with the ruler overlay a height value is denoted. This value is then offset to set the y value at this point to 0 since the starting height of the platform is set and will be added in MATLAB script. These values will then be compared to the simulated behaviour with the largest part of the difference being assigned to camera parallax. Using the least sum of squares to determine this camera parallax, the real placement of the ruler compared to the PM in the direction of the camera view will be determined. For the measurement of the ball again first the data is extracted by frame-by-frame analysis with the overlay, for the ball specifically the top of the ball. The start value of the ball will also be set to the set starting height of the platform, this value will then be reduced by the parallax magnitude based on the ball measurement with the ruler distance from the platform measurement.

B. MATLAB Model

To model the platform motion first the programmed rotor position and velocity are looped and used to fill an array, starting with a velocity of 0 rad/s, a position of 0 rad and a constant acceleration of 1083 rad/s^2. To fill this array in a loop equation 3.4 followed by equation 3.5 are used. This loop has two exclusions, equation 3.1 does not have the i-1 term on i=0 and equation 3.2 will not get used in the final loop. To model the change of direction of the acceleration there are If-statements in the loop, that upon reaching specific timesteps. The first timestep, used to start reverse acceleration, is equal to the time between sending the movement commands to the motor in the measurement.

$$P_r(i) = P_r(i-1) + v_r(i)\delta t + a_r(i)\delta t^2 \tag{3.1}$$

$$v_r(i+1) = v_r(i) + a_r(i)\delta t \tag{3.2}$$

$$A_d = A_{so} - S_r\theta \tag{3.3}$$

This array with rotational rotor positions is then converted to an array with translational movements with pinion radius and subtracted from the starting position of the arm (Equation 3.3). The resulting position of the arm is then converted to the height of the platform using equation 2.3, which results in the platform position.

C. Energy balance

Another way to determine whether the system would be able to launch the ball and high it would travel would be to calculate the energy the motor has put out and dividing this over all the moving components. This would result in a kinetic energy stored in the ball on launch, which can then be converted to height energy. To make a simplified model dependent on the radius of the driving pinion (S_r), the system properties found in table 1 are required.

Motor torque (τ)	Motor acceleration (a_m)	drive efficiency (γ)	PM weight (M_p)	Ball weight (M_b)	Rotor height (h)	Rotor radius (r)	Steel density (d)	Operational distance (s_o)
0.035 Nm	2000 rad/s^2	0.5	20 g	3 g	8 mm	1.25 cm	7850 kg/m^3	1.37 cm

Table 1: Parallel manipulator and motor properties

This model is very simple but will indicate what the ideal pinion radius (S_r) is and how it compares to the chosen radius (S_{rw}). The model ignores the velocity translation and assumes it to be a ratio of 1.0 since the operation takes place between $\pi/3$ and $\pi/6$ at which the ratio is 1.0. For the drive efficiency 0.5 has been selected due to it being the worst efficiency in the operating range. The motor's force is also set constant since the torque speed curve is not yet available for the multi axis stepper. Therefore, the force is set to 0.035 Nm, assuming it to be half of the holding torque of 0.07 Nm.

The first step to determine the relation between the arm velocity and the rotational kinetic energy stored in the rotors, and kinetic energy stored in the platform and ball. To determine the rotational inertia of the three rotors summed first the rotor mass with equation 3.4 and for the inertia equation 3.5 is used.

$$M_r = 3dV = 3\pi d r^2 h \tag{3.4}$$

$$I_r = 0.5 M_r r^2 \tag{3.5}$$

Then the energy output of the motor is approximated over the distance of the operating range (S_o) of the arm with the force as τ/S_r in equation 3.6.

$$E_{tot} = \frac{\tau}{S_r} s_o \gamma \tag{3.6}$$

This energy is then divided over the kinetic energies of the platform and the rotor resulting in a velocity dependent on the pinion radius (S_r). The rotational inertia uses the angular velocity instead of the linear velocity ($\omega = v/S_r$) of the arm. Combined with the kinetic energy in the platform sums to E_{tot} this results in equation 3.7. It must be noted that M_p is a combination of the platform and arm weights for simplification. For just the vertical movement of the platform and ball the weight would be 6 g, this means that the energy of moving the platform and ball up to the launch position would be 0.81 mJ of potential energy compared to the total energy of 8 to 25 mJ dependent on S_r with values of 30 to 10 mm respectively.

$$E_{tot} = E_{rot} + E_{kin} = 0.5(M_P + M_b)v^2 + 0.5 I_r \frac{v^2}{S_r^2} \tag{3.7}$$

$$v = \sqrt{\frac{\tau S_r s_o \gamma}{0.5(M_p + M_b)S_r^2 + 0.5 I_r}} \tag{3.8}$$

Using the result from equation 3.7 to find the time taken to cover the operating range which can then be used to find acceleration this force would achieve if the motor acceleration would be constant as is done in equation 3.9.

$$t = \frac{s_0}{0.5v} \tag{3.9}$$

This time is then used to find the acceleration as a function of the spindle radius (Sr) in equation 3.40.

$$a = \frac{v}{\frac{s_o}{0.5v}} = \frac{v^2}{2s_o} = \frac{\frac{\tau S_r s_o \gamma}{0.5(M_p+M_b)S_r^2+0.5I_r}}{2s_o} = \frac{0.5\tau S_r \gamma}{0.5(M_p + M_b)S_r^2 + 0.5 I_r} \tag{3.40}$$

If the motor acceleration (a_m) multiplied by the radius S_r is lower than the acceleration of the arm (a) as stated in equation 3.40 the system will be limited by the motor acceleration. If the acceleration of the motor is higher than the acceleration of the arm according to equation 3.40 then the system will be limited by the motor force.

To find the highest release velocity the radius with the highest acceleration has to be selected, limited by both the motor acceleration (a_m) and the maximum acceleration determined from the

motor force (a). With the values from table 1 this results in figure 10, showing the acceleration limited by both the motor force (unlimited acceleration) and the motor acceleration (unlimited force).

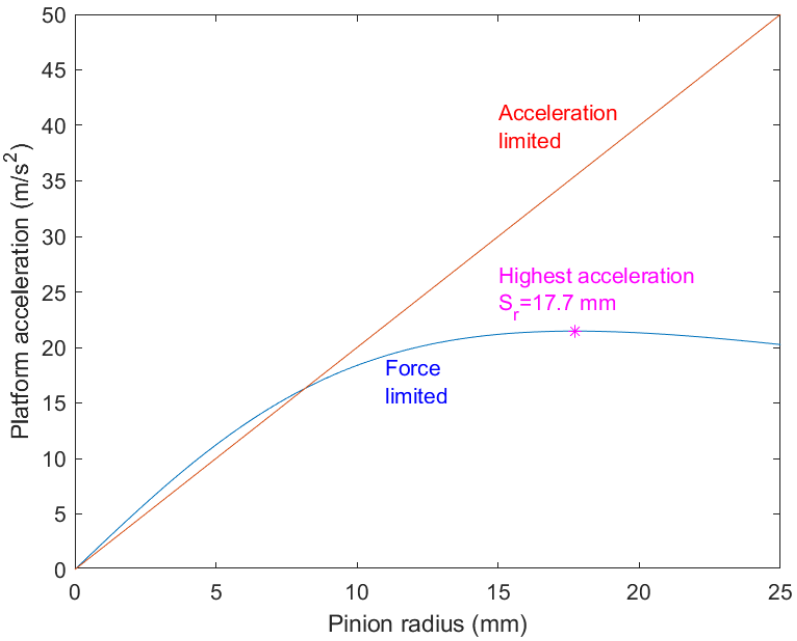

Figure 10: Acceleration of the platform vs Pinion radius, showing the force limit (blue) and the motor acceleration limit (red). Magenta star shows the optimum pinion radius.

With the optimal radius (S_r) of 17.7 mm the velocity results in 0.77 m/s at release (equation 3.8). With this velocity the kinetic energy of the ball can be calculated and converted to gravitational potential energy. The resulting maximum height the ball could achieve with an S_r of 17.7 mm is 30 mm.

IV. Results and discussion

A. Platform position

The result of the least sum of squares determined the placement of the ruler to be 1.23 cm behind the centre of the parallel manipulator. The camera parallax based on this value is shown in Figure 12, with on the right axis the magnitude of the parallax adjustment, this is a relative adjustment. Since the centre of the camera lies above the platform top the parallax is highest at the lowest heights, this is then added to the measurement to compensate for the offset. However, after the parallax compensation the start value is set to the same calculated start height as the

simulations, which causes the parallax error to result in a relative error with the highest subtraction in the centre of the motion.

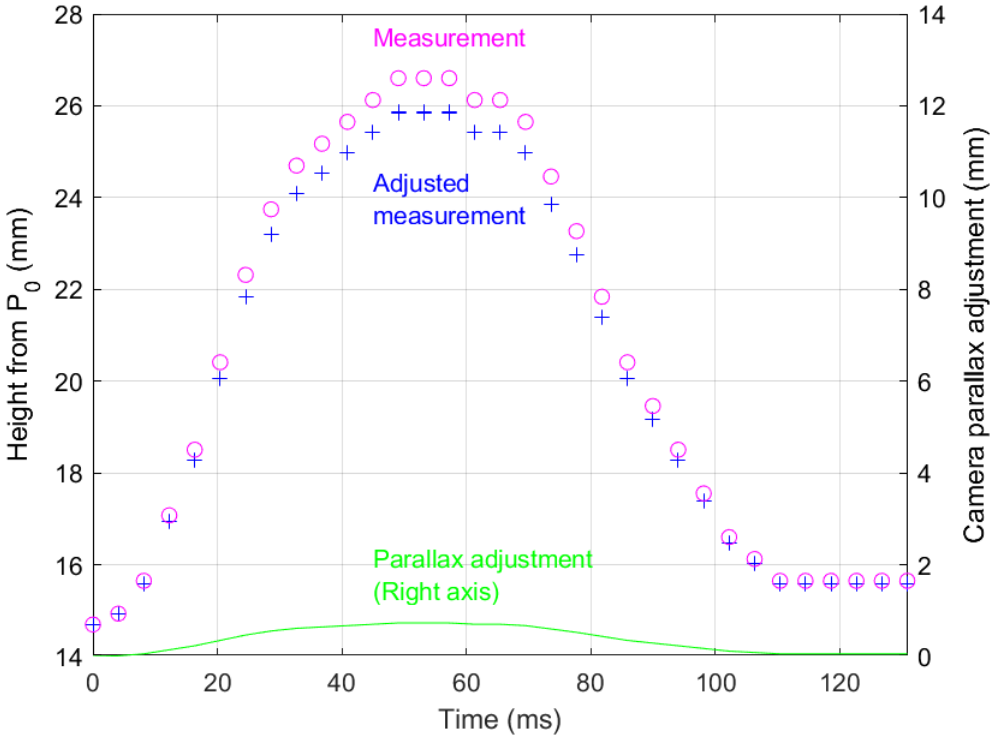

Figure 11: Measured platform height as a function of time (magenta circles) and parallax correction (blue crosses). The parallax correction is at most 1 mm at the top position of the platform (green line).

The parallax adjusted measurement of the platform, compared to the simulated platform can be seen in Figure 12. The Figure 11lso shows the border until which the least sum of squares samples run, this to focus on the initial launch related platform motion. It also shows that the behaviour of the simulated platform fits in the measurement and its error in the launch region, indicating an acceptable simulation. At the top of the simulation the measurement starts to deviate from the model, this however should not influence the launch of the ball. Something to consider is that in the measurement error there could be a steeper curve, providing the ball with a higher release velocity, or a vertical offset which would give a higher release velocity.

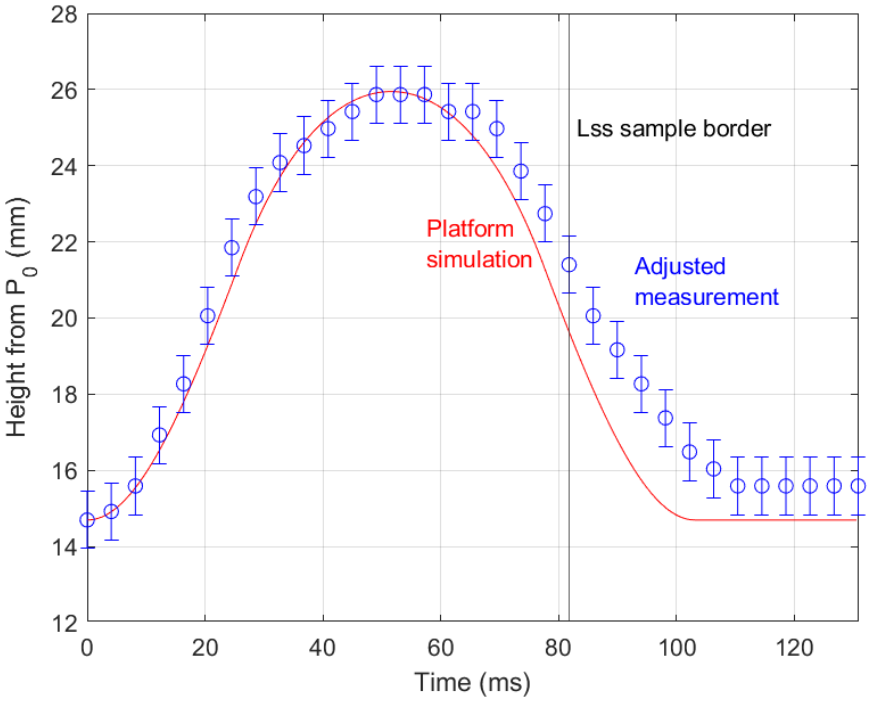

Figure 12: Parallax corrected platform height as function of time compared to the predicted position (red curve). The model predicts the upward movement (first 60 ms) within measurement error. The downward movement is however about 10 ms later than predicted.

B. Platform velocity and acceleration

The platform velocity is what determines the vertical distance the ball will travel after it has been released from the ball. Shown in Figure 13 are the velocities of the platform. The model in red, this is determined by the difference of two adjacent data points over the timestep. For the measurement this is determined by plotting the derivative of a function fit to the data. The measurement's velocity shows a slightly higher peak, which could point to a slightly higher launch distance for the ball. The reverse acceleration of the measurement also shows a more defined curve, which is only slightly present in the modelled velocity. This could be accentuated by the MATLAB polyfit.

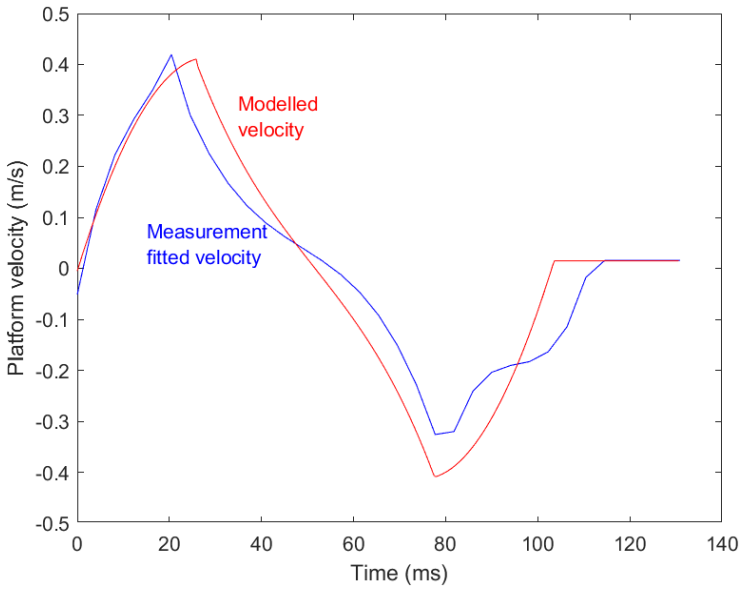

Figure 13: Velocity of the measured platform (blue) and the velocity of the modelled platform (red), showing that the measured platform peaks and reverses earlier and has a slightly higher top than the modelled platform.

The acceleration of the platform is what determines whether the ball can release from the platform. With the ball having a reverse acceleration from gravity of -9.81 the platform should at least dive with this acceleration after launch. In Figure 14 the acceleration of the simulated platform can be seen, with its reverse acceleration between 25 ms and 78 ms the ball should be able to release from the platform since the platform's acceleration magnitude is larger than that of gravity.

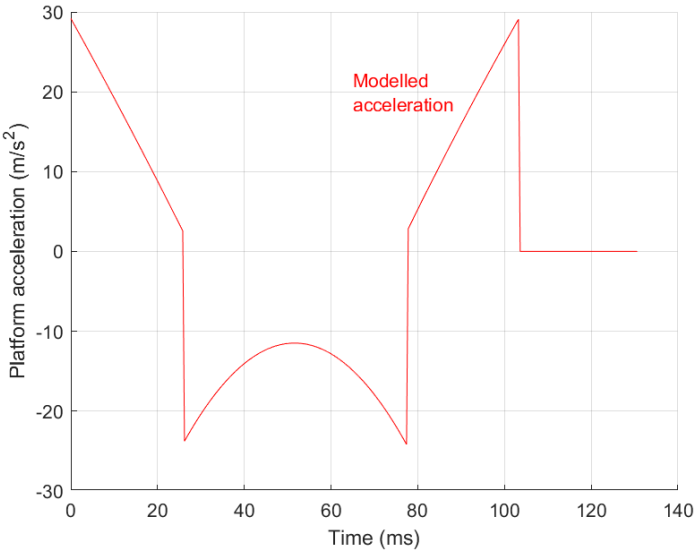

Figure 14: Acceleration of the modelled platform, showing that the platform during its decline (25 - 78 ms) accelerates downwards faster than the ball accelerates downwards (9.81 m/s^2). The second derivative of the measurement was deemed too noisy for use.

C. Ball trajectory

The measurement parallax of the ball can be seen in Figure 15 (green line), with the measured trajectory (magenta circles) and the parallax adjusted measurement of the ball (blue crosses). The ruler distance determined by the platform measurement is also used for these parallax values. With the ball's height difference from the centre of the image being larger the parallax also has a larger magnitude, with a maximum at the top of the ball's trajectory of 2 mm.

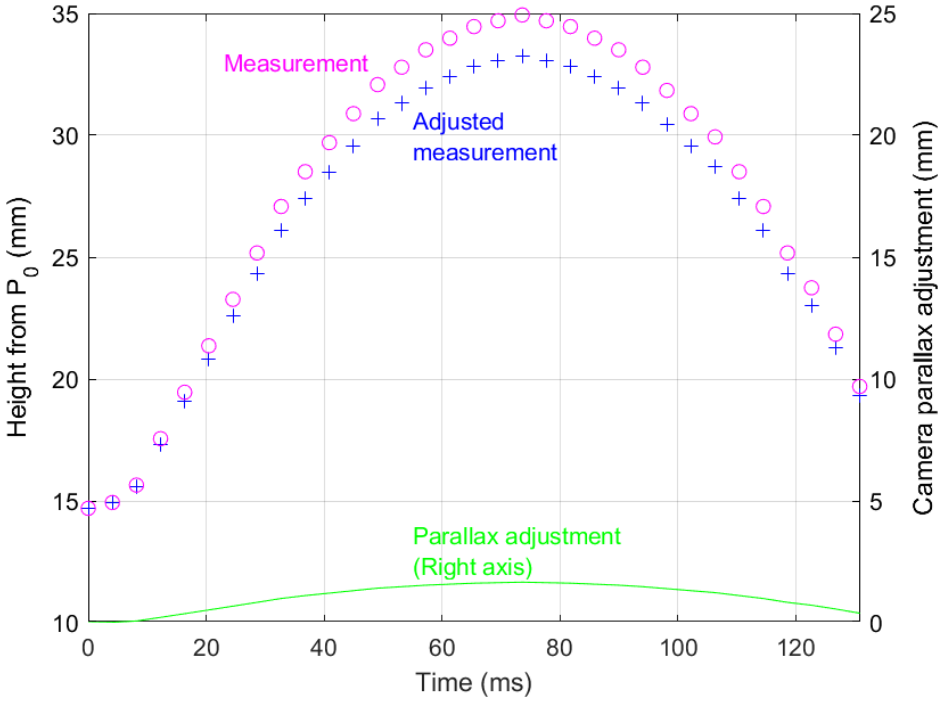

Figure 15: Measurement ball height as a function of time (magenta circles) and parallax correction (blue crosses). The parallax correction is at most 2 mm at the top position of the ball (green line).

As can be seen in Figure 16, the ball measurement outperforms the ball simulation, after the first 10ms the trajectory of the measured ball starts to deviate and has a higher velocity. Plotting the points of release (magenta stars) of the measurement and the ball shows that the measurement and simulation do release at equal height. This indicates that the acceleration as a function of height as modelled does match the real world. The measurement however achieves this point about 4 ms earlier with a higher velocity, which could cause the 4 mm higher top of the measured trajectory compared to the model.

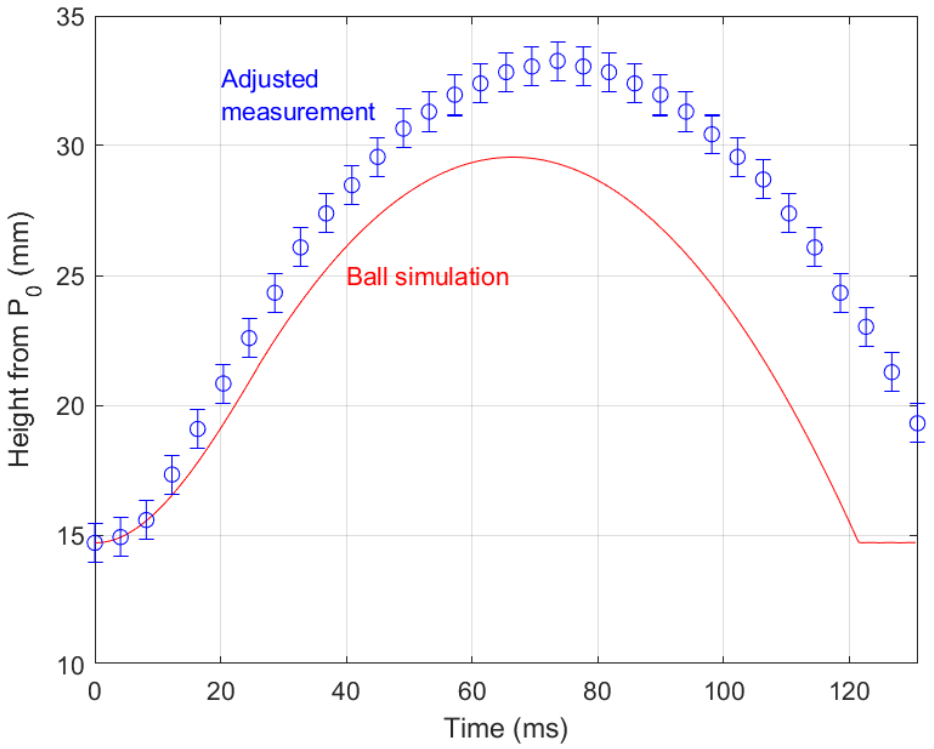

Figure 16: The parallax corrected ball height (blue circles) as a function of time compared to the predicted ball position (red curve). The model only matches the measurement shortly after the start (first 10 ms), after which the velocity of the measurement lies higher than that of the model.

D. Simulated versus measured launch

Figure 17 shows the complete picture of the modelled platform motion versus the measured platform position and the modelled ball trajectory versus the measured ball trajectory. The model launching the ball 7 mm and the measurement launching the ball 11 mm points towards an error, and with the points of release plotted in Figure 14 showing the launch heights being equal the difference should be in the launching velocity as seen in Figure 13. Within the measurement errors in Figure 14 fits a platform position curve that could have the required velocity to launch the ball along the measured trajectory, this platform would have a higher acceleration than the current model has or starts at a slightly more extended rack increasing height gain of the platform over time.

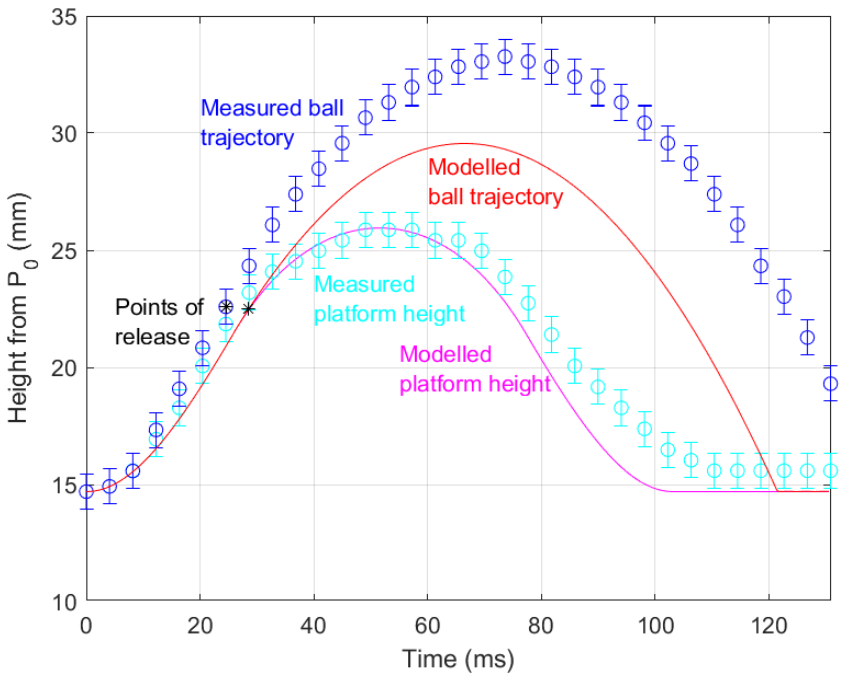

Figure 17: Combining all the graphs shows both the simulated and measured launch. The graph shows that the measurement launches the ball 11 mm while the model launches its ball 7 mm. The points of release (magenta stars) have the same height confirming the acceleration as function of time; however, the measurement is about 4 ms earlier and has a higher release velocity. The measurement shows a peak about 3 mm higher than the measurement predicted.

E. Energy model

Following from the energy calculations is the height achievable at a specific pinion radius, determined to be 30.0 mm. This is calculated with a radius (S_r) of 17.7 mm and table 1 and is compared to a launch with the pinion radius of 10 mm (S_{rw}) chosen in the physical design. With a radius of 10 mm the predicted launch height would be 25.7 mm according to equation 3.8 and the potential energy and kinetic energy equations. Comparing the top position the ball achieved on its trajectory, 11 mm, to the predicted 25.7 mm results in a difference of 14.7 mm. This is a rather large difference of ~60% and indicates that the energy model is incomplete, and that energy is lost to an unmodelled component such as the height energy stored in the ball and platform during the motion before launch or the rotational motion of the arms or the gears. Other slight errors could be caused by either the drive efficiency being set constant at its minimum of 0.5, or that the motor at the lower velocities could have a higher torque than 0.03 Nm. This model does indicate that there is an optimum that likely requires a larger gear radius than 10 mm.

V. Discussion

For many of the measurements the timestep for the data point is crucial to retrieve the velocity of the platform. Therefore, the measurements should have been done with a timekeeping device in frame, this to verify the advertised 240 frames-per-second of the used measuring device. The camera could have also been tested for its behaviour in different light settings. Another thing to consider it whether 240 frames-per-second is enough to extract a nice acceleration curve, in our measurement there was too much noise to retrieve a nice acceleration curve.

Besides the time aspect of the measurement the setup itself could have been more precise, measuring for example the platform and the arms at the same time for comparison and confirmation of the right starting offset of the arms in the model.

The measurement error of the measurement (Figure 12) itself is also rather significant compared to the values of the measurements themselves, allowing to plot a platform path through them that could result in a higher launch velocity. Which could magnify the peak in Figure 13 and explain the difference in the ball's top position.

The radius of the pinion could've been calculated before creation of the physical version of the PM using the motors output energy. For this a model too simple was used however, and the top of the measured ball's trajectory resulted in less than half the height of the modelled top position with the specifications in table 1. The energy calculations do point towards a radius for the pinion (Sr) that could have improved real life launch height. But improving this model the optimal is required if the real optimal value is to be found.

VI. Conclusion

A tri-glide PM has been designed and 3D printed to function on top of a multi axis stepper motor. This 3-DOF PM with 1 translational and 2 rotational degrees of freedom is created to find out what the platform acceleration and velocity achieved by the tri glide are and whether this is sufficient to launch a ping pong ball.

The analysis of the measurement is complicated by the parallax caused by the camera setup. The parallax correction for the platform is 1 mm at its top, and for the ball it is 2 mm at the top of its trajectory. The position of the platform and ball have been modelled. The modelled position of

the platform predicts its behaviour within measurement error for the first 60 ms, however the downward motion is later than the model by about 10ms. For the ball the model is only able to predict the first 10 ms, after which the model is considerably off and predicts a lower velocity. The model is able to predict the release height but with the lower velocity the resulting trajectory reaches a top 3 mm lower than the measured position off the ball. The acceleration of the platform is also key in releasing the ball, the simulated platform acceleration clearly shows an acceleration magnitude high enough to dive under the ball. From the energy calculations can be concluded that with a larger pinion radius the ball would have been launched higher and that a better model is needed to say more.

Leading to the conclusion that the PM was able to launch the ball, but that the model was insufficient to predict the trajectory of the ball or the exact position of the platform.

References

[1] Groenhuis, V., Rolff, G., Bosman, K., Abelmann, L., Stramigioli, S., "Multi-Axis Electric Stepper Motor","IEEE Robotics and Automation Letters 6(4),9484841, pp. 7201-7208"

[2] Arockia Selvakumar, A., Arul Kumar, M., "Experimental investigation on position analysis of 3 - DOF parallel manipulators","Procedia Engineering 97, pp. 1126-1134"

[3] Carretero, J.A., Nahon, M.A., Podhorodeski, R.P.,"Workspace analysis and optimization of a novel 3-DOF parallel manipulator","International Journal of Robotics and Automation 15(4), pp. 178-188"

[4] 'Gan, D., Tsagarakis, N.G., Dai, J.S., Caldwell, D.G., Seneviratne, L.', 'Stiffness design for a spatial three degrees of freedom serial compliant manipulator based on impact configuration decomposition', 'Journal of Mechanisms and Robotics 5(1), pp. 11002-1-11002-10'

[5] 'Cazalilla, J., Vallés, M., Valera, A., Mata, V., Díaz-Rodríguez, M.', 'Hybrid force/position control for a 3-DOF 1T2R parallel robot: Implementation, simulations and experiments','Mechanics Based Design of Structures and Machines 44(1-2), pp. 16-31'

[6] 'Ng, C.C., Ong, S.K., Nee, A.Y.C.','Design and development of 3-DOF modular micro parallel kinematic manipulator','International Journal of Advanced Manufacturing Technology 31(1-2), pp. 188-200'

[7] 'Raj, N.J., Iyer, K., Dash, A.K.', 'Design, fabrication, kinematic analysis and control of a 3-DOF serial manipulator', '2016 International Conference on Next Generation Intelligent Systems, ICNGIS 2016 7854020'

[8] 'Arockia Selvakumar, A.','A numerical approach for 3 PRS parallel manipulator','International Journal of Engineering and Technology(UAE) 7(4), pp. 90-94'